Aqueous Hydrogen Sulphide in Slit-Shaped Silica Nano-Pores:

Confinement Effects on Solubility, Structural and Dynamical Properties

Sakiru B. Badmos and Alberto Striolo*

Department of Chemical Engineering
University College London
London, WC1E 7JE, UK

David R. Cole

School of Earth Sciences
The Ohio State University
Columbus, Ohio 43210, USA

ABSTRACT

Confinement in nm-size pores affects structural and transport properties of water and co-existing volatile species. It has for example been reported that confinement can enhance the solubility of gases in water. We report here equilibrium molecular dynamics simulations for aqueous H_2S confined in slit-shaped silica pores at 313K. We investigated the effect of pore width on the H_2S solubility in water. We quantified the molecular distribution of the fluid molecules within the pores, the hydration structure for solvated H_2S molecules, and the dynamical properties of the confined fluids. The results show that confinement reduces the H_2S solubility in water, and that the solubility increases with pore size. Our analysis suggests that these results are due to perturbations on the coordination of water molecules around H_2S due to confinement. Confinement is found to dampen the dynamical properties of aqueous H_2S as well. Comparing the results obtained for aqueous H_2S to those, reported elsewhere, for aqueous CH_4 we conclude that H_2S permeates hydrated slit-shaped silica nano-pores faster than CH_4. These observations contribute to understand fluids in the subsurface, and could have important implications for applications in catalysis and perhaps for developing new natural gas sweetening technologies.

* Author to whom correspondence should be addressed:
Email: a.striolo@ucl.ac.uk
Phone: +44 (0) 20 7679 3826

INTRODUCTION

Natural gas is widely considered as a high quality, clean and economical energy source. However, produced natural gas can contain undesirable substances such as hydrogen sulphide (H_2S) and carbon dioxide (CO_2). H_2S is of special interest because of its high toxicity, its tendency to corrode pipelines and other equipment,[1] its ability to form clathrate hydrates,[2-3] which can plug pipelines, and to deactivate industrial catalysts.[4-5] It has been reported that the presence of acid gases including H_2S, as well as CO_2 impurities, strongly affect many sub-surface phenomena, including water-rock geochemical reactions with consequences for the optimal strategies for carbon sequestration technologies.[6] The removal of sour gases from natural gas is done industrially by gas-liquid absorption-stripping processes using amine-based compounds,[7] membrane separations,[8] and adsorption.[7, 9] In a theoretical study from our group,[10] it was suggested that hydrated nanopores show large selectivity to H_2S permeation, compared to other typical natural gas components. This manuscript seeks to quantify the molecular mechanisms responsible for our prior observation.

Silica-based porous materials are widely used as representative substrates for academic investigations because silica is one of the most abundant materials on Earth. Because the results from such studies can improve applications such as separations,[11] nanofluidics,[11] catalysis,[12] environmental remediation,[13] and sub-surface geo-energy,[14] many investigations focused on structural and dynamical properties of fluids confined in silica nanopores of varying pore size[15] and different morphologies.[11, 16-18]

This article considers guest molecules adsorbed in confined water. The structural and dynamical properties of confined water is strongly affected by the confining pore surfaces;[19] it is expected that this effect dictates the behavior of guest molecules adsorbed within the hydrated pore.

The solubility of volatile gases in different solvents under confinement is receiving increasing attention.[20-25] Several studies reported an enhanced solubility of gases in liquids confined in small pores, a phenomenon referred to as 'oversolubility'. For example, Luzar and Bratko[24] found enhancement of the solubility of N_2 and O_2 in water by 5-10 folds when confined in hydrophobic pores of width 38-43Å. The enhanced solubility of gases under confinement has been confirmed experimentally.[26-27] Pera-Titus et al.[26] studied the solubility of H_2 in $CHCl_3$, CCl_4, n-hexane, ethanol and water when confined within γ-alumina, silica and MCM-41, and found that H_2

solubility was enhanced by up to 15 times the corresponding bulk value when the pore size is less than 15nm. Rakotovao et al.[27] confirmed the results of Pera-Titus et al. using ^{1}H NMR. A study from our group[20] revealed higher solubility of methane in water when the latter is confined in a partially filled 1nm-wide silica pore. Ho et al.[21] reported enhanced CO_2 and H_2 uptake in a MCM-41 pore containing octamethylcyclotetrasiloxane (OMCTS). Hu et al.[15] reported oversolubility of methane in confined benzene, and discussed how such solubility depends on pore width. Gadikota et al.[28] recently reported the solubility of CH_4, CO_2, and argon in water confined within Na-montmorillonite pores. Using both experiments and simulations, these authors demonstrated greater solubility for CO_2 and Ar in confined water compared to bulk water, whereas results for CH_4 suggest that confinement in montmorillonite pores reduces solubility.

According to Ho et al.,[21] oversolubility could be due to one, or several of the following mechanisms: (i) the solute interacts more strongly with the surface than the solvent, favoring its adsorption close to the pore walls; (ii) the pore is partially filled, resulting in gas/solvent interface which facilitates adsorption of the gas into the solvent-rich phase; and (iii) the solubility follows a confinement-induced mechanism where adsorption of the gas is favored in regions of low solvent densities generated due to layering of the solvent. Our results[20] regarding the enhanced solubility of methane in confined water seem to be due to the second and third phenomena. A balance between solute-substrate, solvent-substrate, and solvent-solute interactions is expected to dictate the resultant oversolubility.[15] Gadikota et al.[28] showed that solute size and the presence of salt in confined water are also important in modulating the free energy of dissolution of various gases in confined water.

H_2S is chosen here because of its relevance to industrial applications, and also because it is a polar substance. Comparing the predicted solubility of H_2S in confined water to that predicted for CH_4 discussed elsewhere,[20] will therefore allow us to better understand the controlling mechanisms. The results will also complement those of Gadikota et al.,[28] who considered both CH_4 and CO_2, a non-polar compound with large quadrupole, in water confined within montmorillonite pores.

We employ molecular dynamics (MD) simulations to investigate the effect of confinement on the solubility of H_2S in confined water. Our analysis documents structural and dynamical properties of the confined fluids. The simulations were

conducted at 313K and pressures in the range of ~ 5 – 26 bar. We focused on the comparison of the properties of the confined fluids with that of the bulk.

The remainder of this manuscript is organized as follows: We first provide a description of the simulation models and algorithms implemented, we present the simulation results, we then conclude by summarizing our main findings.

2 SIMULATION METHODS AND ALGORITHMS

2.1 Simulation set up

2.1.1 Pseudo-bulk systems

To calculate the solubility of hydrogen sulphide (H_2S) in water, as well as the interfacial tension of the liquid-vapor interface we conducted equilibrium molecular dynamics simulations for a biphasic system in the canonical ensemble (NVT). The protonation state of H_2S in all simulations reported here is consistent with low pH. Our simulations were conducted at 313K. The initial configuration was built by placing a thick slab of 400 water molecules in a simulation box of dimension 19.6Å x 19.6Å x 30Å. The water slab was first equilibrated in canonical ensemble for 1ns and then centered in a tetragonal periodic cell of 19.6Åx 19.6Å x 90Å, where it was allowed to come in contact with H_2S vapor. H_2S molecules were placed in the vapor phase on both sides of the water slab as shown in **Figure 1a**. The simulation setup is similar to what has been described in literature.[29-30] The number of H_2S molecules was varied to manipulate the pressure of the system. The number of water molecules was kept constant. The pressure of the system was calculated from the H_2S density above the water slab using the Peng-Robinson equation of state.[31] The compositions of the systems simulated and the corresponding bulk pressures are shown in **Table 1**.

To study the solvation of H_2S in bulk liquid water we conducted additional simulations, in which no interfaces were present. The composition for these simulations was taken from the solubility simulations, the simulation box was cubic with size of 40Å x 40Å x 40Å, and periodic boundary conditions were implemented in all 3 directions. The canonical (NVT) ensemble was implemented.

Table 1: System composition with corresponding bulk pressures for bi-phasic simulations used to estimate H_2S solubility in bulk water and the interfacial tension.

Bulk Phase System	Composition (molecules)	Bulk Pressure (bar)
1	$8H_2S$-$400H_2O$	5.5±0.5
2	$18H_2S$-$400H_2O$	10.9±0.7
3	$24H_2S$-$400H_2O$	14.0±0.3
4	$32H_2S$-$400H_2O$	18.9±0.7
5	$40H_2S$-$400H_2O$	22.6±0.6

Confined systems

The silica substrates used in this study were obtained from β-cristobalite SiO_2 by cutting the crystal along the (1 1 1) crystallographic plane. Placing two silica slabs parallel to each other with a separation distance d (i.e., the pore width), creates the slit-shaped pores. The distance d is the shortest center-to-center distance between the oxygen atoms of the -OH groups on the silica surface measured across the pore volume along the Z-direction. Consistent with low pH conditions, all non-bridging oxygen atoms were protonated, resulting in -OH surface density of 4.54 per square nanometer. This is in reasonable agreement with experiments.[17] Each silica slab is parallel to the X-Y plane of the simulation box and has dimensions of 104.05 x 100.8 $Å^2$. The silica slabs were kept fixed throughout the simulation except the hydrogen atoms on the surface, which were allowed to vibrate. The X and Y dimensions of the simulation box are kept fixed for all simulations at 224.78Å and 100.8Å, respectively, while the Z dimension changes depending on the pore width. The Z dimensions of the simulation box are 42.92Å, 47.80Å and 54.92Å for 1nm, 1.49nm and 2.2nm pores, respectively. The simulation box is periodic in X, Y and Z directions, but the silica slab is only periodic along the Y direction as it is exposed to two bulk regions along the X direction (see Figures 1b and 1c). The simulation setup is similar to the one implemented in previous studies reported by our group.[20, 32]

The initial configuration for the 1.0 nm-wide pore was obtained by first placing 6,000 water molecules in the unconfined region of the simulation box. A simulation was then conducted for 3 ns to allow the water molecules to adsorb within the pore. The 6,000 water molecules fully fill the 1nm pore and yield a thin water film near the pore entrances. H_2S molecules were then placed in the unconfined volume on both sides of the silica pore. As the simulation progresses, H_2S molecules exchange between the

hydrated pore and the bulk. At equilibrium, H_2S molecules occupy the bulk region as shown in **Figure 1b**, and a few H_2S molecules adsorb in the hydrated pore. The bulk pressure of the system is estimated from the H_2S density calculated along the X-direction using the Peng-Robinson equation of state.[31] The errors in the estimated bulk pressure are due to H_2S density fluctuation in the unconfined volume on both sides of the silica pore. The H_2S solubility was calculated by studying the water-H_2S composition in the pore. The pressure of the system was manipulated by changing the number of H_2S molecules in the bulk volume. Similar procedures were implemented to study pores of different widths. The corresponding system compositions and bulk pressures are shown in **Table 2**.

2.2 Force fields

The rigid SPC/E model was used to describe water as it gives reasonable estimates for structure, density, and diffusion coefficient of liquid water at ambient conditions.[33] The potential model developed by Kamath and Potoff was used to describe H_2S.[34] The CLAYFF force field was implemented to model the silica slabs.[35] CLAYFF is a general force field widely used for simulating fluids interacting with clay and clay-related substrates. Non-bonded interactions were modeled by dispersive and electrostatic interactions. The dispersive interactions were described by the 12-6 Lennard Jones (LJ) potential, while the electrostatic interactions were described by the Coulombic potential. The LJ parameters for unlike atoms were obtained using Lorentz-Berthelot combination rules.[36] The cut off distance for all interactions was set to 9Å. The long-range corrections to electrostatic interactions were implemented using the Particle Mesh Ewald (PME) method.[37]

Table 2: Confined system composition (number of molecules) with corresponding bulk pressures. Note that three pore widths were considered.

Pore width: 1nm		**Pore width: 1.49nm**		**Pore width: 2.2nm**	
Composition $H_2S - H_2O$	Bulk pressure (bar)	Composition $H_2S - H_2O$	Bulk pressure (bar)	Composition $H_2S - H_2O$	Bulk pressure (bar)
120-6000	5.2±0.1	200-7600	7.4±0.2	300-10000	9.1±0.4
240-6000	10.4±0.2	400-7600	14.4±0.3	500-10000	14.6±0.3
360-6000	14.9±0.3	600-7600	20.5±0.3	700-10000	20.1±0.5
600-6000	23.0±0.4	800-7600	26.0±0.6	900-10000	24.2±0.5

2.3 Algorithms

All simulations were performed using the simulation package GROMACS, version 5.1.2[38-39] in the canonical ensemble (NVT). Newton's equations of motion were solved using the leapfrog algorithm.[40] The temperature of the system was maintained at 313K using the Nose-Hoover thermostat[41-42] with a relaxation time of 100fs. The water bonds and angles were kept fixed using SETTLE algorithm.[43] For bulk and pseudo-bulk simulations, each system was equilibrated for 18ns, followed by a production run of 12ns conducted for data analysis. Because analysis of density fluctuations suggested that 100ns of equilibration runs are needed for systems involving silica substrates, those simulations were conducted for a total time of 120 ns, with the last 10 ns used for data analysis. The system was considered equilibrated when H_2S densities fluctuate around constant values, and the system energy fluctuates within 10% of its average values.

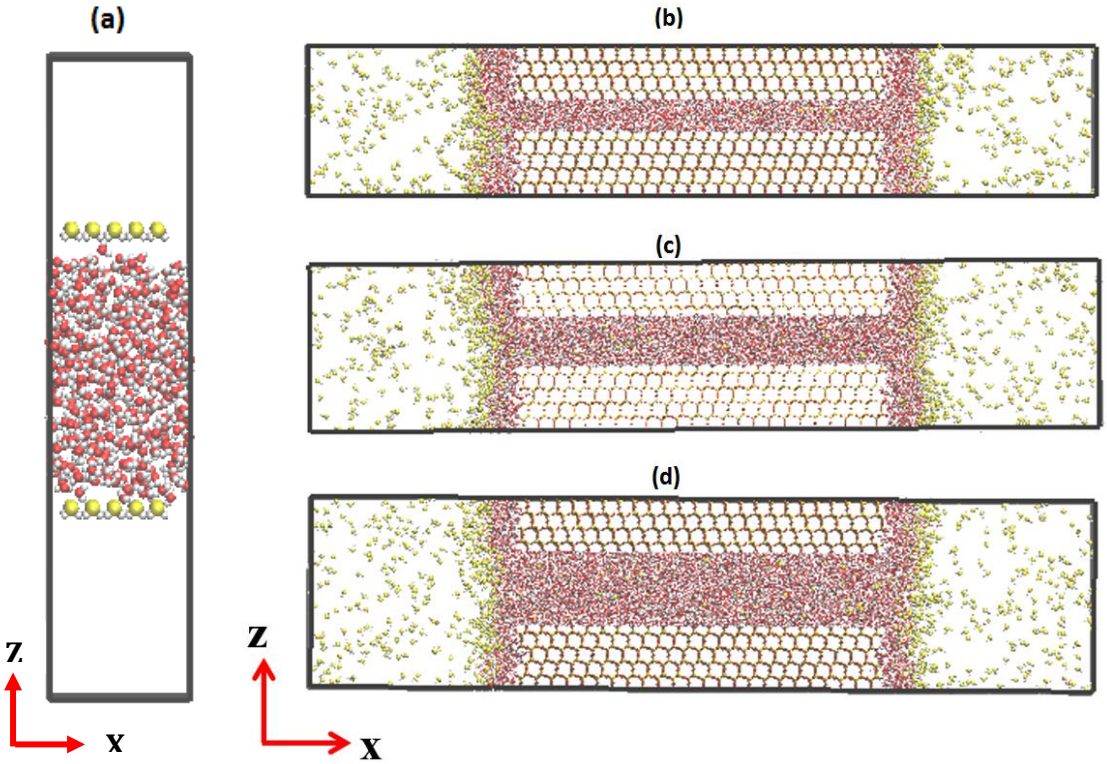

Figure 1: The initial configuration for the pseudo-bulk simulation containing 400 molecules of water and 40 molecules of H_2S is shown in panel (a).The simulation snapshots of the simulated pores are shown in panels (b-d). The pore widths are (b) 1nm (c) 1.49nm (d) 2.2nm. For the fluid molecules, oxygen atoms are shown in red, Sulphur atoms in yellow and hydrogen atoms in white.

3 RESULTS AND DISCUSSION

3.1 Pseudo-bulk systems

The atomic density profiles of water oxygen (OW) and sulphur of H_2S (S) for biphasic simulations of compositions shown in **Table 1** are reported in **Figure 2**. The Z direction is perpendicular to the liquid water slab. The results are expressed in number density for both OW and S. In the gaseous phase the density is low, as expected, while in the liquid phase the density is consistent with that of bulk liquid water at 313 K. The solubility of H_2S in bulk water is estimated as the ratio of the average number density of S to the average number density of OW in the liquid slab. The portion of the slab used for the solubility calculation is located within points A and B shown in **Figure 2**, to exclude the two interfaces. The simulated results as a function of pressure are reported in **Table 3**. The uncertainties in the estimated pressures reflect density fluctuations in the gaseous phase. Comparison of the solubility results against the experimental data reported by Kuranov et al.[44] is provided in **Figure 3**, top panel. It is clear that the force fields implemented here under-estimate the solubility of H_2S in bulk water and that the discrepancy increases as the pressure increases. The under-estimation of the solubility in water could be a consequence of the fact that the H_2S force field implemented here was developed for pure H_2S. The mixing rules implemented here may not adequately represent the physical interactions between H_2S and water. The experiments of Kuranov et al. were chosen to compare our simulation data because they were obtained at similar thermodynamic conditions as those chosen for our simulations. Other, less compatible experimental data for H_2S solubility in water are available.[45-49] While at low to moderate pressure ($P < 5$ bar) the experimental results by different groups are in agreement,[45,48] the agreement deteriorates as the pressure increases. For example, Selleck et al.[46] suggested that H_2S solubility in water increases rapidly as pressure increases, while Gillespie et al.[49] do not agree with this trend. Rather than attempting to resolve this argument, our simulations provide benchmark data for H_2S solubility in bulk water to quantify the effect of confinement.

To validate the force fields against experimental data, as well as to assess whether our implementation of the simulation algorithms was reliable, we quantified the effect of H_2S on the interfacial tension (IFT) of water, γ. The IFT γ is estimated using: [50]

$$\gamma = \frac{1}{2} L_z \left[\langle P_{zz} \rangle - \frac{1}{2} \left(\langle P_{xx} \rangle + \langle P_{yy} \rangle \right) \right] \quad (1)$$

In Eq. (1), L_z is the length of the simulation box along the Z-direction, perpendicular to the interface, while P_{xx}, P_{yy} and P_{zz} are the pressure tensors along X, Y and Z directions. The ITF results are presented in

Table 3 and in **Figure 3**, panel b. The simulated IFT data are in reasonable agreement with experiments,[51] as shown in **Figure 3b**. The slight difference between simulated and experimental IFT data could be due to the truncation of the dispersive interactions, which were not corrected for in our calculations.[52] For completeness, the IFT of pure SPC/E water at 313K has been reported to be 60.7 mN/m[53] while in our simulations (not discussed for brevity) we obtained 55.1±1.8 mN/m. Both simulated and experimental results show that H_2S decreases the water surface tension, and that the effect is stronger as the H_2S pressure increases. Because the density profiles of **Figure 2** suggest an accumulation of H_2S at the interface, our simulations suggest that H_2S acts as a surfactant, consistent with what has been reported by Riahi and Rowley.[29] According to Riahi and Rowley[29], contacting a slab of water simulated with the polarizable model SWM4-NDP at the density of 764kg/m^3, with liquid H_2S of density 764kg/m^3 at 313K reduced the IFT from 63 mN/m to 20 mN/m, which is in good agreement with experimental data. [51]

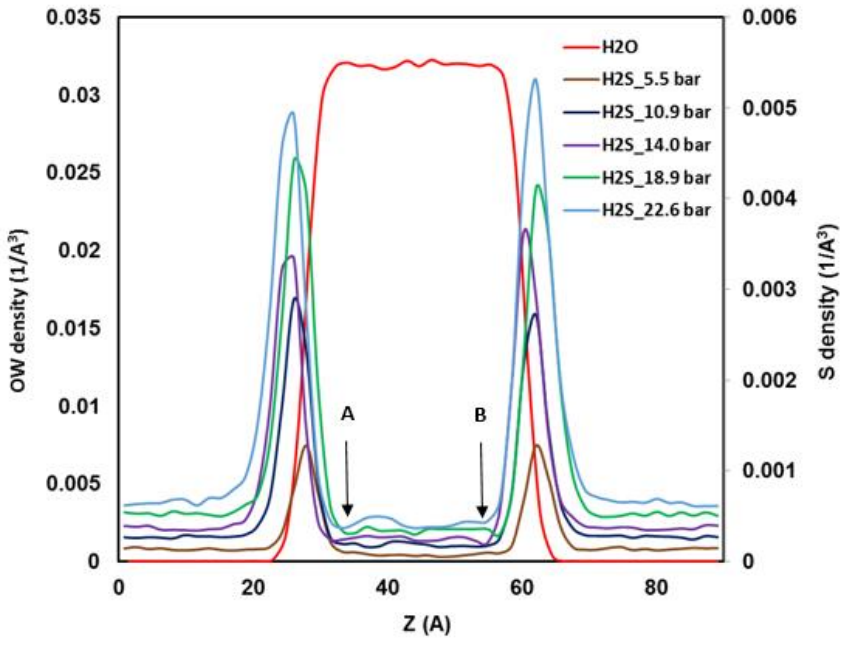

Figure 2: Density profiles of sulphur of H_2S (S) and oxygen atom of water (OW) along the Z direction of the simulation box at different bulk pressures. Figure 1, panel

a, presents the schematic simulation set-up used for these simulations. Only one profile is shown for OW because it does not change significantly with pressure.

Table 3: Solubility of H_2S in water and water interfacial tension (IFT) at different bulk pressures.

Bulk Pressure (bar)	**H_2S solubility x 10^3**	**IFT (mN/m)**
5.5 ± 0.3	4.3 ± 1.1	52.1 ± 1.6
10.9 ± 0.7	6.9 ± 1.0	47.8 ± 1.4
14.0 ± 0.4	8.1 ± 0.4	46.7 ± 1.3
18.9 ± 0.7	11.0 ± 1.2	43.8 ± 1.6
22.6 ± 0.6	13.2 ± 0.8	42.2 ± 1.8

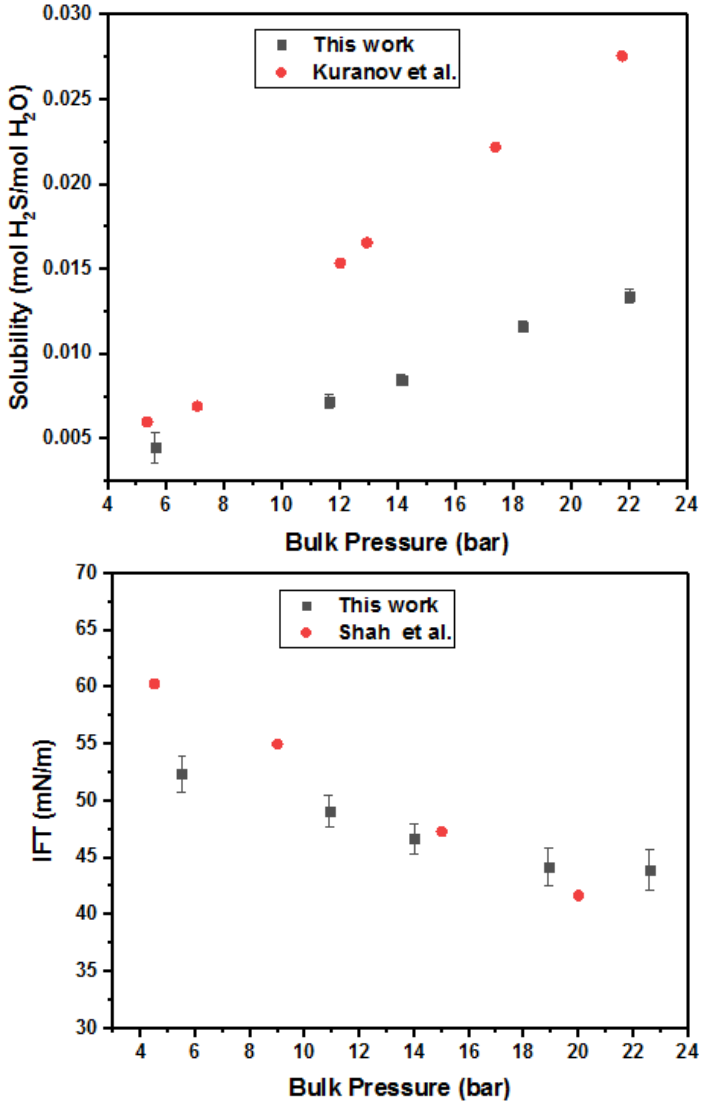

Figure 3: Comparison of simulated data against experiments from literature. (a) Simulated solubility of H_2S in water compared against the experiments of Kuranov et al.[44] (b) Simulated water interfacial tension (IFT) compared against the experimental

data of Shah et al.[51] In both cases the results are shown as the pressure of H_2S increases. In the simulations, the errors were estimated as standard deviation from the mean.

To quantify the solvation of H_2S molecules in bulk liquid water we also conducted an equilibrium simulation for bulk systems, in the absence of interfaces, as described in the Methods section. The system comprises 2123 H_2O molecules and 3 H_2S molecules, mimicking the solubility at ambient conditions. The simulation was conducted at atmospheric pressure and 313 K. To quantify the hydration structure we calculated the radial distribution function (RDF) between the sulphur (S) of H_2S and the oxygen of water (OW), as well as the RDF between S and the hydrogen atoms of water (HW). The results are in good agreement with the ab-initio study performed by Riahi and Rowley,[29] who used the CP2K package.[54] We also calculated the 3 dimensional distribution of oxygen atoms of water (OW) around the bulk H_2S. The results are shown in **Figure 4**. This system was also used to compute the self-diffusion coefficient of both water and H_2S in the bulk. The values obtained were 3.2 ±0.8 and 3.5 ±0.5 x 10^{-9} m^2/s for H_2S and water, respectively, which are consistent with the simulated values in the literature.[29, 55] The estimated diffusion coefficient of H_2S in water is in reasonable agreement with the value of 2.6±0.1 x 10^{-9} m^2/s reported by Riahi and Rowley,[29] who conducted simulations using polarizable force fields. Tamimi et al.[56] reported experimental diffusion coefficients for H_2S in bulk water. At 308K, the reported value was 2.55 x 10^{-9} m^2/s.

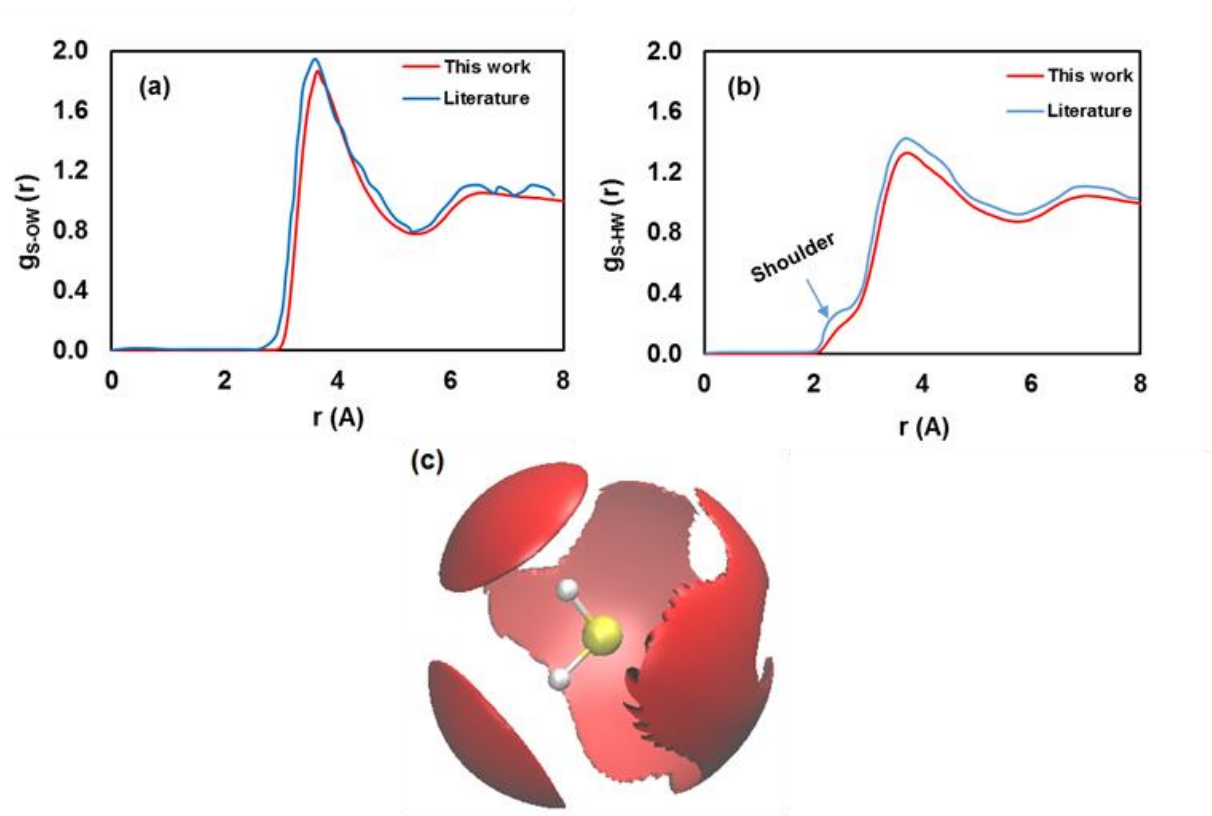

Figure 4: Hydration structure of H_2S in bulk water at atmospheric conditions. (a) Radial distribution function between sulphur (S) of H_2S and oxygen of water (OW) , (b) Radial distribution function between sulphur of H_2S and hydrogen atoms of water (HW), (c) 3D distribution of OW around H_2S. The iso-density surface is drawn at 0.363Å^{-3}. In panels (a) and (b) the literature data sets are from Riahi and Rowley.[29] The arrow in panel (b) highlights a shoulder discussed in the text.

3.2 Confined systems

3.2.1 Density profiles

The distribution of molecules within the 1.0 nm – wide pore is quantified in terms of molecular density profiles in the direction perpendicular to the pore surfaces. The density profiles for water oxygen atoms (OW) and sulphur atoms of H_2S (S) are shown in **Figure 5** at different H_2S pressures. Because the density profile of OW does not change significantly with H_2S pressure, only one such profile is shown for clarity. For all profiles shown, the position Z=0 is the center of the pore. For the 1 nm – wide pore, +5Å and -5Å represent the location of oxygen atoms of the –OH groups on the two silica surfaces across the pore volume. The OW density profiles reveal layering of water molecules with two distinct hydration peaks formed at a distance of ~1.25Å from the pore walls. This suggests that water molecules interact strongly with the pore surfaces, possibly through hydrogen bonds, as discussed in detail elsewhere.[57]

The results reveal that H_2S molecules distribute primarily in the region close to the pore center while they seem excluded from the interfacial region. The exclusion of H_2S from the regions near pore walls could be due to the limited ability of H_2S to form hydrogen bond with the -OH groups on the surface, as well as to the large water density near the interfaces, which could yield steric hindrance. The difficulty of H_2S to form hydrogen bonds was attributed by Riahi and Rowley to its large size and weak polarity.[29] The small shoulder in the RDF between bulk S and HW supports the limited ability of H_2S to form hydrogen bonds with water (see **Figure 4b**).

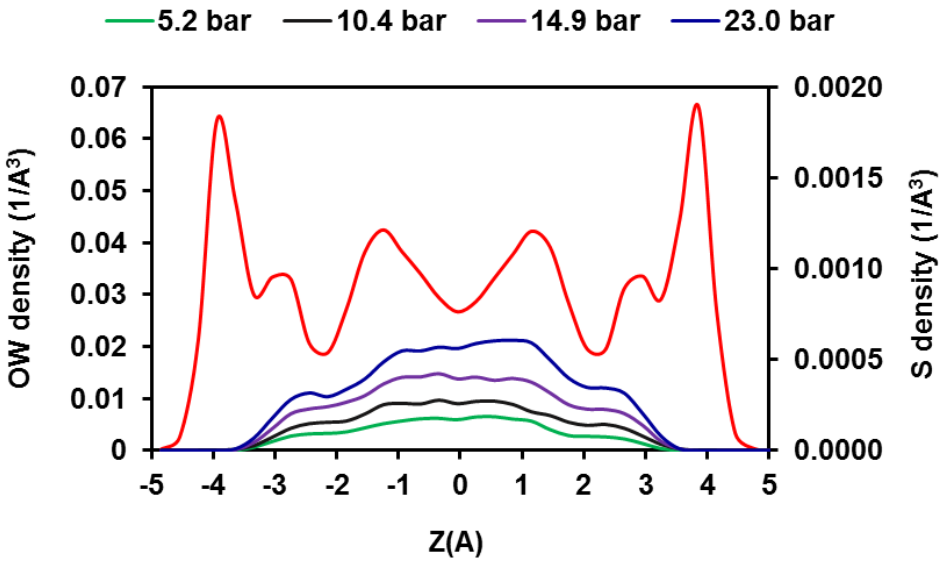

Figure 5: Density profile of oxygen atoms of H_2O (OW, red line) at 23 bar and sulphur atom of H_2S (S) along the direction perpendicular to the pore surface at different bulk pressures for a 1nm slit pore.

3.2.2 Solubility

The solubility of H_2S in water confined within the 1.0 nm – wide pore is estimated as the ratio of the number of H_2S adsorbed at equilibrium to the number of water molecules within the pore. To eliminate pore entrance effects, we excluded ~ 1 nm portion from the pore entrances. The results, reported in

Table 4 and in **Figure 6**, show that the solubility of H_2S in confined water increases as the bulk pressure increases, but in all cases, it is much lower compared to the solubility in bulk water.

Table 4: Solubility of H_2S in confined water for all simulated pores. The errors are standard deviations from the mean obtained from 5 blocks of production simulations, each of which lasts 2ns.

Pore width: 1nm		**Pore width: 1.49nm**		**Pore width: 2.2nm**	
Bulk Pressure (bar)	Solubility x 10^3	Bulk Pressure (bar)	Solubility x 10^3	Bulk Pressure (bar)	Solubility x 10^3
5.2 ± 0.2	3.0 ± 0.5	7.4 ± 0.2	3.7 ± 0.2	9.1 ± 0.4	5.1 ± 0.8
10.4 ± 0.2	3.7 ± 0.7	14.4 ± 0.3	6.9 ± 0.4	14.6 ± 0.3	7.5 ± 0.6
14.9 ± 0.4	5.1 ± 0.6	20.5 ± 0.3	9.9 ± 0.5	20.1 ± 0.5	10.4 ± 0.5
23.0 ± 0.4	8.1 ± 1.0	26.0 ± 0.6	10.5 ± 1.5	24.2 ± 0.5	13.8 ± 0.5

The observation that confinement reduces H_2S solubility in water is contrary to most studies that indicate solubility increases in confinement.[20, 22-24] However, in some cases it has been reported that solubility decreases upon confinement.[28, 58] For example, Hu et al.[15] reported lower solubility for methane in benzene confined within graphite pores for pore width in the range ~16-32Å. For CO_2, a non-polar molecule with large quadrupole, Ho et al.[22] reported enhanced solubility in water confined in ZSM-5, MCM-41, and MIL-100 nano-porous materials. Our results suggest that for water-H_2S in the 1.0 nm – wide silica pore, there is no preferential adsorption of H_2S close to the pore walls and no fluid-fluid interface is available inside the pore as the pore is fully hydrated. H_2S adsorption does not occur where local water density is low, suggesting that there is no enhancement of H_2S density via a bulk-like solubility mechanism. Thus it appears that none of the mechanisms leading to oversolubility described by Ho et al.[21] takes place for the system considered here. For completeness, it should be mentioned that Ho et al.[21] considered the solubility of H_2 gas in OMCTS confined in MCM-41. They observed accumulation of H_2 in the pore center, where the OMCTS density was low.

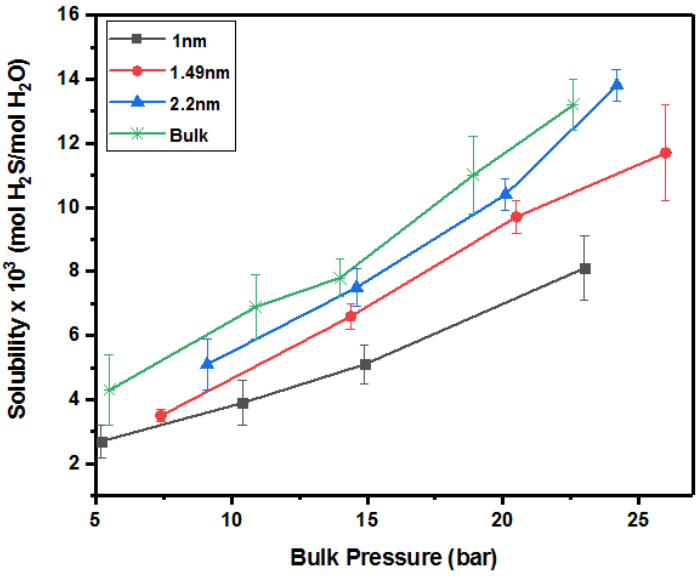

Figure 6: H_2S solubility in water versus bulk pressure. The simulation results are shown for bulk water and for water confined in all pore sizes considered here. Lines are only guides to the eye.

3.2.3 H_2S hydration structure

To investigate whether the lower solubility of H_2S in confined water is related to its hydration structure, the atomic radial distribution function was determined between sulphur of H_2S and oxygen of water ($g_{S\text{-}OW}$) along with the 3D spatial distribution function (SDF) of the oxygen atoms of water molecules within the first hydration shell of H_2S. Note that in all the simulations for the 3D SDF analysis, the H_2S molecules are free to move. For these calculations we used the MD-Analysis code,[59-60] implemented in an in-house Python algorithm. The radius of the first hydration shell corresponds to the position of the first minimum in $g_{S\text{-}OW}$. To obtain these data, an independent simulation was conducted within one 1 nm – wide pore without the bulk regions. The X and Y dimensions of this simulation box are 104.78 and 100.82Å, respectively. Due to periodic boundary conditions, the pore is effectively infinite along X and Y directions. This simulation was conducted for 30 ns, the last 4 ns of which were analyzed. The composition of the confined system represents the equilibrated hydrated pore exposed to H_2S at a pressure of 23 bar (see **Table 5** for the composition of the simulated system). We chose 23 bar because it was the largest pressure considered here. The RDF and SDF for the confined system are compared to analogous datasets obtained for a bulk system simulated at 23 bar and 313K. It should be noted that a 2 dimensional in-plane RDF was calculated for the confined system

since the pore surfaces confine the system along the Z-direction, while 3D RDF was calculated for the bulk system. The results are presented in **Figure 7**.

The RDFs in **Figure 7a** show a higher first peak for the bulk system than for the confined system, while the position of the peak is similar. This suggests a stronger hydration of bulk H_2S. These results are consistent with the SDF of water oxygen atoms within the hydration shell of H_2S, shown in **Figure 7b** and **Figure 7c**. These data suggest that bulk water is able to provide a more complete hydration structure to H_2S than water confined in the 1.0 nm – wide silica pores considered here.

Although confinement reduces H_2S solubility in water, while it enhances CH_4 solubility as reported elsewhere,[20] our results show that H_2S solubility in confined water is higher than that of CH_4. This comparison holds despite the fact that the study on CH_4 solubility was conducted at 300K, a lower temperature than simulated here, and at pressures higher than those considered here.

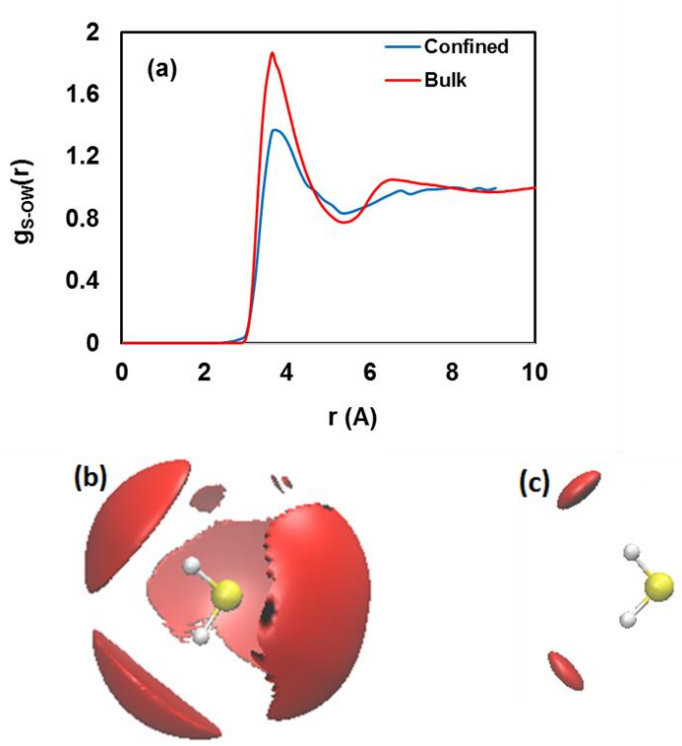

Figure 7: (a) Radial distribution function between Sulphur atom of H_2S and water oxygen in the 1.0 nm – wide pore (blue line) and in the bulk (red line); (b) 3D spatial distribution function (SDF) of water oxygen atoms in the first hydration shell of H_2S in bulk water; and (c) confined in a 1 nm – wide pore. The iso-density surfaces are drawn at 0.364Å^{-3} and 0.303Å^{-3} for bulk and confined water, respectively. For computational reasons it was necessary to consider slightly different iso-density surfaces. The results clearly show that OW is much less dense in the hydration structure of confined H_2S.

3.3 Effect of pore size

To investigate how the solubility of H_2S in confined water changes with pore size, we simulated additional silica nano-pores of width 1.49 nm and 2.2 nm. The atomic density profiles for OW and S are shown in **Figure 8**. The density profiles for OW do not change significantly as the pressure increases. Our results reveal that the height of first and second hydration layers, LO1 and LO2 in **Figure 8**, are similar for both pore sizes. This suggests that the pore hydration structure does not change significantly with pore width for the pores considered here. For the two pores considered in **Figure 8**, our results show that the water density near the pore center approaches the value expected for bulk liquid water (0.033 molecules $Å^{-3}$). Our results also show layering of H_2S molecules, with the formation of a pronounced H_2S layer (LS1) near the position of the second hydration layer (LO2). The H_2S density increases as the pore size increases from 1.49 nm to 2.2 nm, and also increases as the pressure increases, suggesting that solubility also increases.

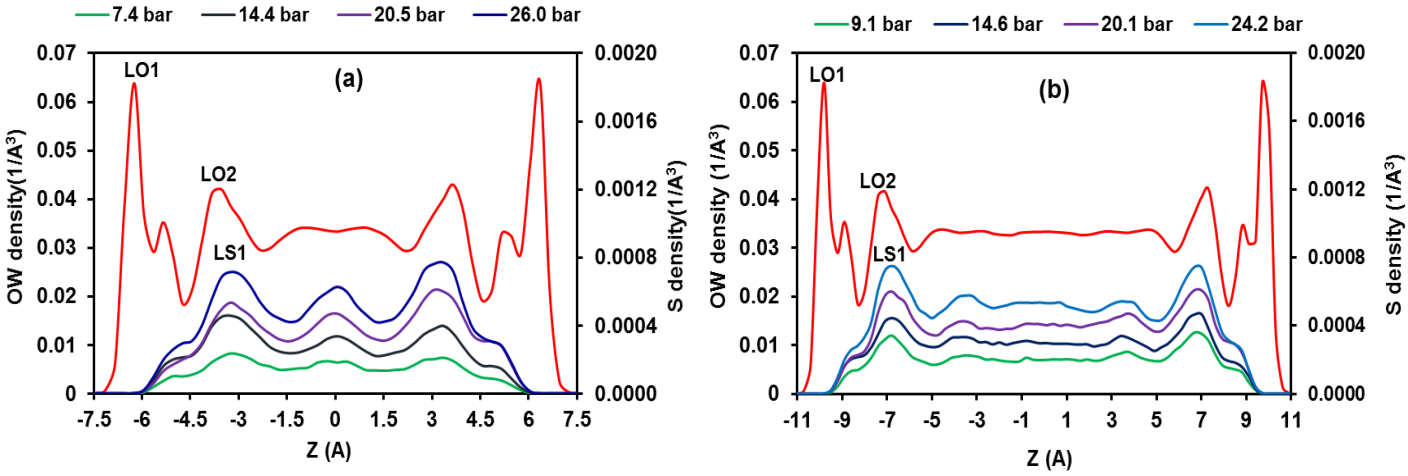

Figure 8: Same as Figure 5 for pores of width 1.49 nm (a) and 2.2nm (b). In both panels LO1 and LO2 denote the first and second hydration layers, respectively, from the silica surface. LS1 denotes the H_2S layer near the second hydration layer. Note that density profiles of oxygen atoms of H_2O (OW, red line) for panels (a) and (b) are at 26.0 bar and 24.2 bar, respectively.

The solubility of H_2S in confined water for all simulated pores is shown in **Figure 6**. The results show that the solubility in confined water at the conditions considered is always lower than that in bulk water, and that it decreases as the pore width decreases. To understand why solubility increases with pore width, we investigate the hydration structure of H_2S in the various environments. For these calculations the water-H_2S

system was confined in effectively infinite pores along the X and Y directions (because of periodic boundary conditions). The simulations were conducted for 30 ns, the last 4 ns of which were used for data analysis. The composition of the systems was chosen to replicate, approximately, the equilibrated systems at 23 bar (see **Table 5**). Note that as the pore size increases, more water molecules are required to fill the pores. The amount of H_2S present within the pores is determined based on the solubility data at 23 bar (see **Figure 6**). While for the 1 nm pore simulation data were available, for the two larger pores the solubility was interpolated based on the simulation results at other pressures. RDF and 3D SDF results are presented in **Figure 9**. Note that RDFs are calculated in 2D for confined, and in 3D for bulk systems.

Table 5: Composition of the fluid systems simulated at 23 bar in pores with period boundary conditions implemented along both the X and Y directions as well as in the bulk.

Pore size (nm)	**Number of H_2O molecules**	**Number of H_2S molecules**
1.00	2875	28
1.49	4680	49
2.20	7140	91
Bulk	2064	58

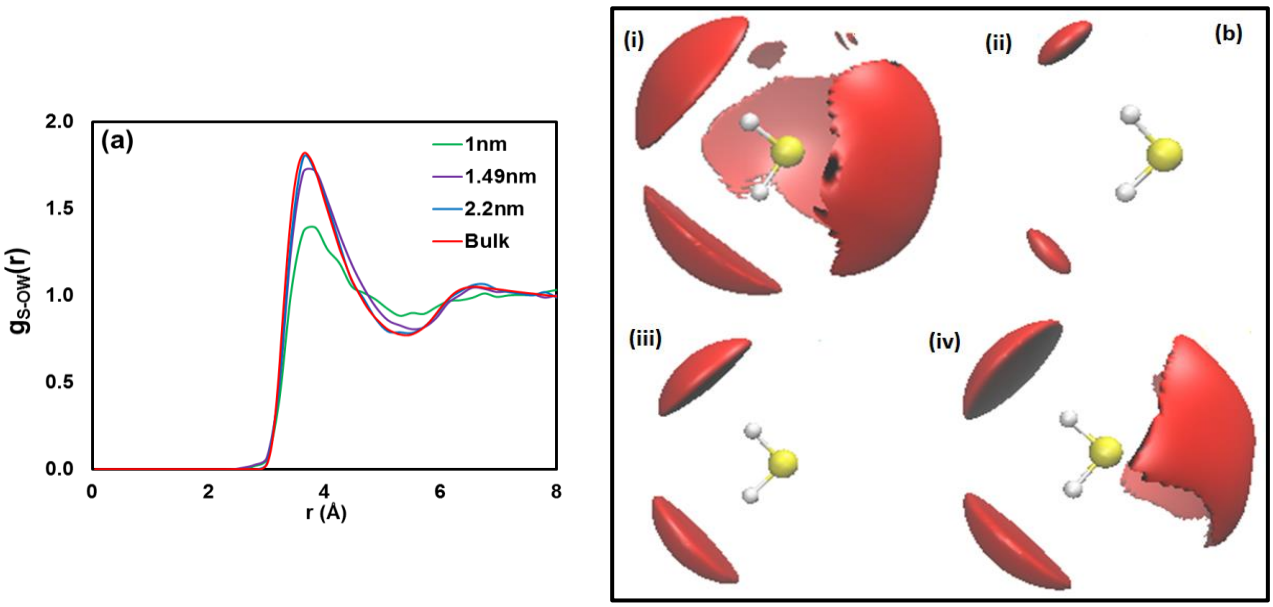

Figure 9: Same as Figure 7, for all systems considered. Panel b shows, the 3D SDF for (i) bulk system (ii) 1nm – wide pore (iii) 1.49 nm – wide pore (iv) 2.2 nm – wide pore. The iso-density surfaces are drawn at 0.364Å^{-3}, 0.303Å^{-3}, 0.318Å^{-3} and 0.345Å^{-3}, respectively. The iso-density surfaces are drawn at different densities for computational reasons.

The first peak in the RDFs is located at the same distance for all systems considered, but the peak intensity is the lowest for the system confined in the 1 nm pore, and the highest for the bulk system. The height of the first peak in the RDF for the 1.49 nm and for the 2.2 nm pore are similar to that for the bulk dataset, but there is a tendency for the peak intensity increases with pore width. These results suggest that the hydration structure for confined H_2S molecules is significantly different compared to the bulk when the pore is of 1.0 nm in width, but as the pore width reaches ~1.5 nm in width the hydration structure is similar to what observed in the bulk. This observation is consistent with the density distributions along the direction perpendicular to the pore surface (see **Figure 4** and **Figure 8**). Note, there is a correspondence between the position of the H_2S peak LS1 with the hydration layer LO2, which is present in pores of width 1.49 and 2.2 nm, but not in the pore of width 1.0 nm. The results are also consistent with the fact that the water density near the center of the 2.2 nm – wide pore is similar to that of bulk liquid water. The 3D SDF results (**Figure 9b**) confirm that the molecular structure within the first hydration shell of H_2S becomes very similar to what observed in the bulk when the pore width is of 2.2 nm, whereas it is significantly different when the pore is of width 1.0 nm.

The results just discussed are consistent with results for the interaction energies between H_2S and water, which were estimated in bulk water as well as in water confined in the various pores. The results (shown in Supplemental Material) reveal that H_2S has the most attractive interaction with water in the bulk and the least in the 1nm pore, consistent with the trend of solubility decrease with decreasing pore width. Our results are qualitatively consistent with those reported for aqueous NaCl reported by Malani et al.[58] This group reported a lower NaCl solubility in water confined within graphene pores of width 0.8 nm compared to bulk water, and that the solubility increased with pore width. The increase in solubility was attributed to increase in the coordination number of water molecules around ions as the pore size changed from 0.8 to 2.0 nm. However, NaCl is a salt, and therefore rather different than H_2S. It is likely that the mechanisms responsible for the reduced solubility in confined water are due to different mechanisms in these two cases.

3.4 Structural properties

3.4.1 Orientation

The density profiles shown in **Figure 8** reveal layering of water molecules and H_2S molecules. The orientation of water molecules in these layers is quantified in terms of the distribution of the angle theta, formed between the dipole moment vector of water and the vector normal to the surface, as well as that of the angle between the H-H vector of water and the vector normal to the surface. We complement this analysis with density profiles of oxygen and hydrogen atoms of water in the direction perpendicular to the surface. The results, presented in Supplemental Material, are consistent with prior investigations of the changes in the properties of interfacial water due to interactions with a silica surface.[11, 57]

The orientation of confined aqueous H_2S molecules is quantified by analyzing the angle formed by the vector S-M, pointing from the sulphur atom to the mid-point (M) of the H-H vector in H_2S, and the surface normal vector, as well as the angle formed by the H-H vector of H_2S and the surface normal vector. The results, shown in Supplemental Material, show that there is no preferential orientation for aqueous H_2S in the 1.0 nm – wide silica pore, nor within the other pores considered here.

3.4.2 In-plane density distributions

We also calculate in-plane density distributions of oxygen atoms of water OW in layers LO1 and LO2, and that of S atoms of H_2S in layer LS1. For these calculations only the pores of width 1.49 and 2.2 nm were considered. In the 1.0 nm pores the layer LS1 could not be identified (see density profiles in **Figure 5**). For the positions of layers LO1, LO2, and LS1 please refer to **Figure 8**. The results for the pore of width 1.49 nm are shown in **Figure 10.** Those for the 2.2 nm are not shown because they do not change significantly compared to those shown in **Figure 10**. The simulations were conducted at 26 bar. The results show an X-Y section of thickness 1.5Å centered on the atomic density peak. The contour plots show a well-structured LO1 hydration layer, in which OW atoms distribute near the vertices of the hexagonal rings formed by the silicon atoms in the solid substrate. This is consistent with what has been observed previously.[11, 57] Water molecules in layer LO2 show a uniform distribution, also consistent with what has been reported previously.[11] The in-plane distribution of H_2S molecules in layer LS1 suggests no preferential distribution, although there may be some aggregation of confined aqueous H_2S.

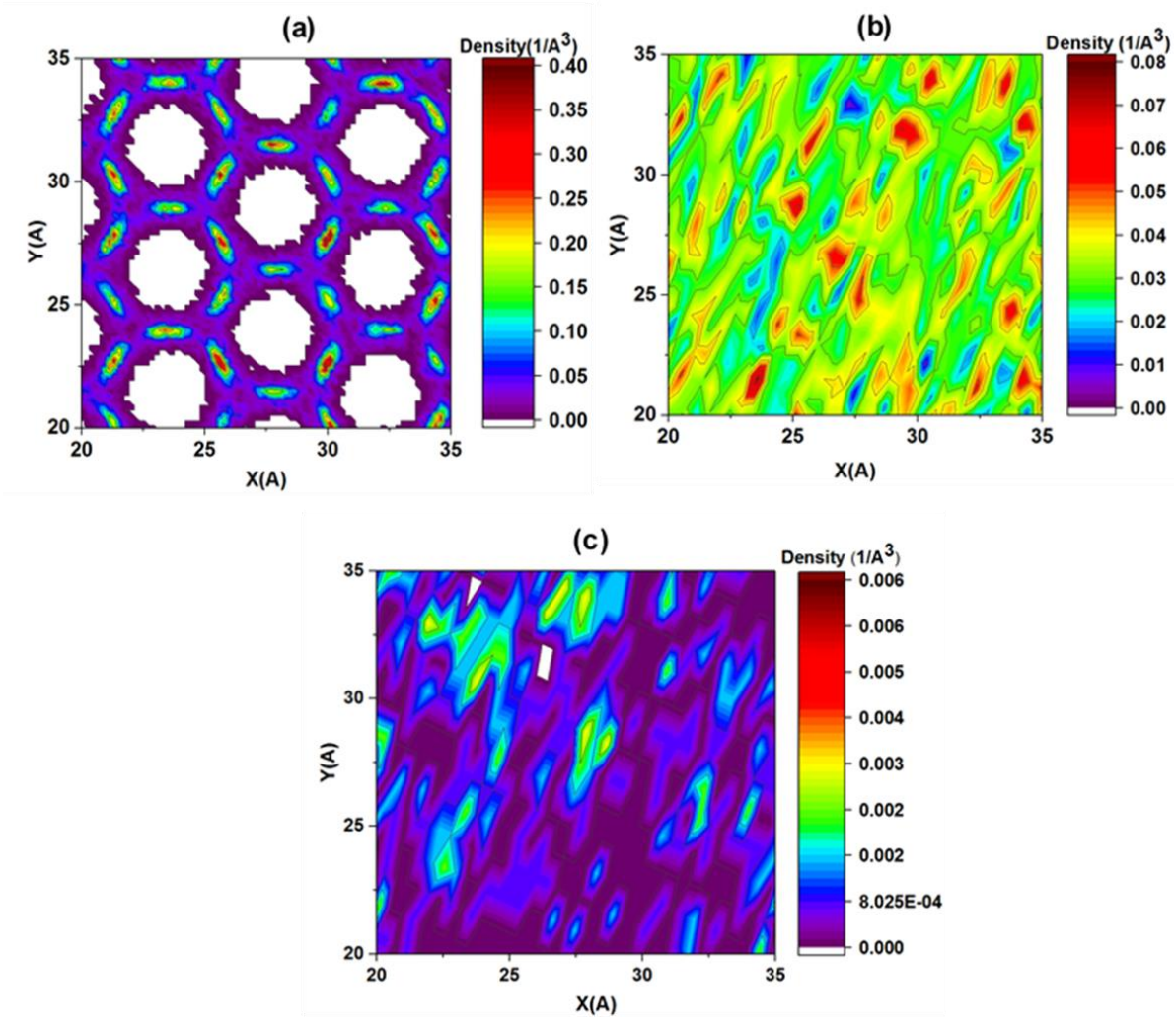

Figure 10: In-plane density distribution of oxygen atoms of water in layer LO1 (a) and LO2 (b). In plane density distribution of sulphur atoms of H_2S in layer LS1 (c). The results are obtained for the 1.49 nm – wide silica pore. The pore contains 800 H_2S and 7600 H_2O molecules. H_2S and 7600 water molecules

3.5 Dynamical Properties

3.5.1 Diffusion Coefficients

To investigate the transport of H_2S through the hydrated pores, we plot its mean square displacement (MSD) as a function of time (see details in Supplemental Material). Three systems were considered for these calculations, whose composition is reported in **Table 5**. From the MSD data the diffusion coefficients were calculated for H_2S and water using the Einstein equation[61]:

$$D = \lim_{t\to\infty} \frac{\langle |r_i(t' + t) - r_i(t')|^2 \rangle}{2Dt} \qquad (2)$$

In Eq. (2), $r_i(t)$ and $r_i(t')$ are the positions of molecule i at time t and time origin t', respectively, and D is the dimensionality of the system. In our systems, D equals 2 for

H_2S in confined water and 3 in the bulk. The calculated diffusion coefficients are shown in **Table 6**.

Table 6: Diffusion coefficients for H_2S in water. The results are shown for the bulk system, as well as for the three confined systems. The bulk pressure is 23 bar.

System	D(H_2S) (10^{-9} m^2/s)	D(H_2O) (10^{-9} m^2/s)
1nm pore	2.2±0.3	1.3±0.2
1.49nm pore	2.4±0.2	1.9±0.3
2.2nm pore	2.7±0.1	2.3±0.2
Bulk	3.0±0.2	3.7±0.2

The results suggest that confinement slows the diffusion of aqueous H_2S. The diffusion coefficient of H_2S is slowest in the 1nm pore. We note that even though this diffusion coefficient is slower than what observed in bulk water, it is ~ 3 times faster than that calculated for hydrated CH_4 in the same pore ($7.83x10^{-10}$ m^2/s).[10] In the case of H_2S in water, confinement only reduces the diffusion coefficient by ~20-30%, while in the case of aqueous CH_4 confinement in the 1 nm – wide silica pore slowed down the diffusion coefficient by ~50-60%. From the results in **Table 6** it is also evident that confinement dampens the diffusion of confined water, which was observed before.[62] It is noteworthy that while in the bulk system the diffusion coefficient of aqueous H_2S is slower than that of water, in confinement the opposite occurs. This is likely a consequence of the fact that water molecules accumulated near the silica surfaces have very slow diffusion.

To quantify whether the diffusion of H_2S through the hydrated pores is isotropic or anisotropic, we extracted positions of H_2S molecules at time t and $t + \Delta t$ ($\Delta t =$ 250ps), from which we calculated two-dimensional XY vectors. The last 20 ns of the simulation were used for this analysis. The end-points of the vectors are shown in Supplemental Material. We then applied the principal component analysis (PCA) method,[63] as described elsewhere,[64] to calculate the eigenvalues and eigenvectors to reduce the datasets. When the eigenvalues are similar, the diffusion in X-Y plane is isotropic; when the eigenvalues are different, the diffusion is anisotropic. The eigenvalues for all the simulated pores are reported in Supplemental Material. The results suggest that diffusion of H_2S in the three hydrated pores is isotropic along X

and Y directions, as was the case for CH_4 diffusion in the hydrated silica pore of width 1 nm.[64]

Knowing both the solubility, S, of H_2S in confined water and its diffusion coefficient, D, through the hydrated pore, we can estimate the permeability, P, using the relation:[65]

$$P = S \text{ x } D \qquad (3)$$

In Eq. (3), P is measured in mol/m·s, S is expressed in mol/m^3, and D is measured in m^2/s. The estimated permeability of H_2S through the hydrated 1nm pore is 8.01 x 10^{-7} mol/m·s. By comparison, the permeability of CH_4 through the same hydrated pore was estimated at 5.63 x 10^{-7} mol/m·s.[10] The difference in permeability is due to the higher solubility and higher diffusion coefficient of H_2S in confined water compared to methane. The larger permeability for H_2S compared to methane supports our prior hypothesis that hydrated nano-pores could function as perm-selective materials for natural gas sweetening.

3.5.2 Residence Times and Rotational Dynamics

The residence times for individual molecules within particular layers within the hydrated pores were calculated from the auto-correlation function C_R (t):[66]

$$C_R(t) = \frac{\langle N_i(t) N_i(0) \rangle}{\langle N_i(0) N_i(0) \rangle} \qquad (4)$$

In Eq. (4), $N_i(t)$=1 if molecule i resides in the layer of interest at time t and 0 otherwise. If molecule i belongs to the layer at time t=0, $N_i(0)$=1 and remains equal to 1 as long as molecule i stays in the layer; but this quantity becomes 0 when molecule i leaves the layer of interest. C_R (t) decays from 1 to 0. The faster C_R (t) decays to zero, the faster the molecules leave the layer of interest. In **Figure 11a** we show C_R (t) for water molecules found within different layers in the 1.49 nm pore size. The results are compared with C_R (t) for bulk water. In the bulk water case, the residence time was calculated as the time, on average, spent by water molecules within a slab of the same dimensions as those considered in the pores. In the simulations considered in **Figure 11** the confined system consists of 800 H_2S molecules and 7600 water molecules, while the bulk system is comprised of 58 H_2S molecules and 2064 water molecules. The thickness of the layers centered on peak

positions in LO1 and LO2, as well as those in the bulk, as considered in **Figure 11**, in all cases is 1.5Å.

Our results show that water molecules in the first hydration layer (LO1 in **Figure 8**) remain within the layer longer than water molecules in layer LO2 and the middle of the pore. When compared with bulk water, water molecules in all regions of the pore show longer residence times. $C_R(t)$ is also computed for those H_2S molecules found in a layer centered on LS1 and of thickness 1.5 Å, which is located at the same location as LO2. The results, shown in **Figure 11b**, show that H_2S has a shorter residence time than the water molecules in the same region. The faster dynamics of H_2S in this region could be due to its limited ability to form hydrogen bonds with water molecules in this layer, and is less influenced by the silica surface.

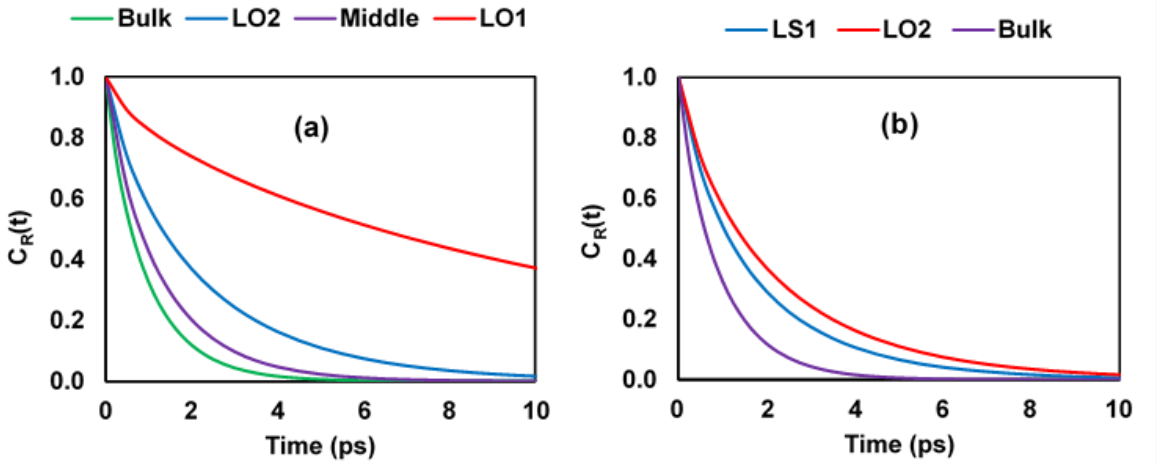

***Figure 11**:* Residence auto-correlation function for water molecules in layers LO1 and LO2 and in the middle of the pore of width 1.49 nm compared to that of bulk liquid water (a). Residence autocorrelation function for water molecules in layer LO2, H_2S molecules in layer LS1, and bulk water molecules (b). The confined system consists of 800H_2S and 7,600 water molecules. The bulk system consists of 58 H_2S and 2,064 water molecules.

The rotational dynamics of the fluid molecules were quantified by calculating autocorrelation functions for the dipole moment of water molecules and the S-M vector for H_2S molecules. The S-M vector is the vector pointing from the sulphur atom to the midpoint (M) of the H-H vector of one H_2S molecule. The vector-vector autocorrelation function is defined as:[66-67]

$$C_v(t) = \frac{\langle v_i(t) v_i(0) \rangle}{\langle v_i(0) v_i(0) \rangle} \qquad (5)$$

In Eq. (5), $v_i(0)$ is either the dipole moment vector or the S-M vector of molecule i at time t=0. We consider the same systems discussed in **Figure 11.** The results, shown in **Figure 12**, suggest that water molecules in layer LO1 rotate more slowly than those water molecules in hydration layer LO2 and slower than bulk water. This agrees with prior simulation results,[11] and confirms that the interactions of hydration water molecules with the silica pore surface slow down the rotation of interfacial water molecules. This effect becomes weaker as water molecules are further from the solid-liquid interface. In **Figure 12** we also report the results for H_2S molecules. When we compare the results for bulk H_2S to those for H_2S molecules in layer LS1, it appears that confinement slows down the rotational dynamics of H_2S molecules, but not very significantly. When we compare the auto-correlation function dataset obtained for H_2S molecules in layer LS1 to those obtained for water molecules in layer LO2, we observe that H_2S molecules rotate much faster than water molecules at this distance from the silica surface. This observation is likely due to the difficulty encountered by H_2S molecules in forming strong hydrogen bonds with water molecules, and is consistent with the residence times results presented in **Figure 11**.

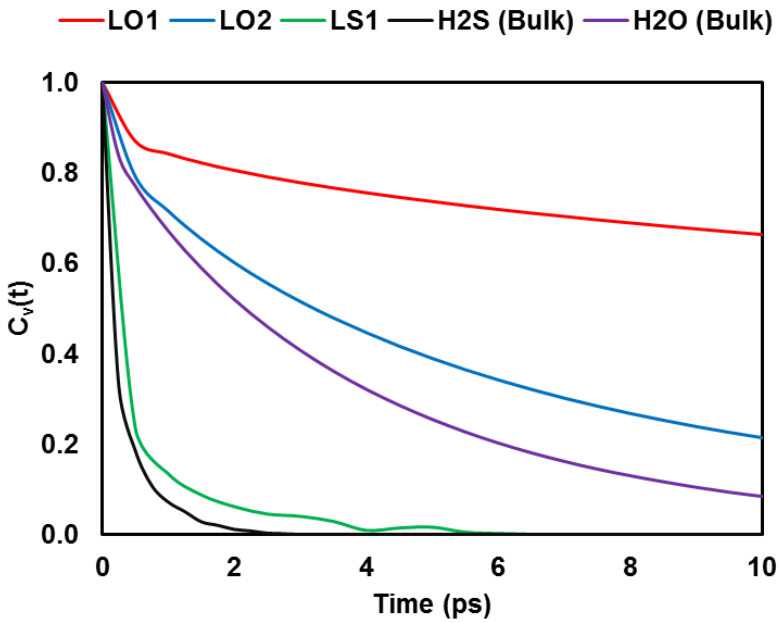

Figure 12: Vector-Vector autocorrelation function for fluid molecules at different regions of the 1.49nm pore compared with that of bulk water. The confined system consists of 800 H_2S molecules and 7,600 water molecules. The bulk system consists of 58 H_2S and 2,064 water molecules.

4 CONCLUSIONS

Atomistic equilibrium molecular dynamics simulations were performed for systems composed of different loadings and ratios of water and H_2S in slit-shaped silica pores of different widths at 313K. The pressure of the system was manipulated by changing the number of H_2S molecules in the pseudo-bulk region. The study was performed to investigate the effect of confinement on the solubility of H_2S in water, as well as on structural and dynamical properties of the confined fluids. The simulation results are quantified in terms of atomic density profiles in the direction perpendicular to the pore walls, solvation structure, as well as dynamical properties including permeability of H_2S across the hydrated 1.0 nm-wide pore. Our results reveal that confinement reduces H_2S solubility in water. Analysis of the hydration structure suggests that confinement strongly affects the ability of water molecules to solvate H_2S molecules when the silica pores are narrower than ~ 1.5 nm. The diffusion coefficients computed for H_2S molecules dissolved in confined water show that confinement reduces the diffusion coefficient, up to ~20-30% in the narrowest pores considered here compared to bulk values. By computing both solubility and diffusion coefficient for H_2S molecules in confined water we could assess its permeability through hydrated pores. The H_2S permeability in a 1 nm – wide silica pore filled with water at 313 K has been found to be higher than that of methane at similar conditions, suggesting the possibility of using hydrated slit-shaped silica nano-pores for natural gas sweetening. In addition, the results presented here improve our understanding of the behavior of fluids in subsurface formations.

Supporting Information

Eigenvalues from principal component analysis on H_2S diffusion in water confined in nano-pores; interaction energy between H_2S and H_2O; probability distribution of angles for H_2S and H_2O; mean square displacements as a function of time. This material can be found free of charge on the ACS Publications website at DOI:

Acknowledgements

Generous allocations of computing time were provided by the National Energy Research Scientific Computing Center (NERSC) at Lawrence Berkeley National Laboratory and the University College London High Performance Facility (LEGION@UCL). NERSC is supported by the DOE Office of Science. S.B.B.

acknowledges financial support from the Petroleum Technology Development Fund (PTDF). A.S. acknowledges financial support from the European Union via the Marie Curie Career Integration Grant No. 2013-CIG-631435. This research received funding from the European Union's Horizon 2020 research and innovation program under Grant No. 640979. D.R.C. was supported by the U. S. Department of Energy, Office of Basic Energy Sciences, Division of Chemical Sciences, Geosciences and Biosciences under grant DE-SC0006878. We are grateful to the group of Dr. Chris Lorenz, in particular Mateusz Bieniek for sharing Python code to complete the 3D spatial distribution analysis.

REFERENCES

1. Tsay, L. W.; Chi, M. Y.; Chen, H. R.; Chen, C. Investigation of Hydrogen Sulfide Stress Corrosion Cracking of Ph 13-8 Mo Stainless Steel. *Mater. Sci. Eng. A* **2006**, *416*, 155-160.

2. Buch, V.; Devlin, J. P.; Monreal, I. A.; Jagoda-Cwiklik, B.; Uras-Aytemiz, N.; Cwiklik, L. Clathrate Hydrates with Hydrogen-Bonding Guests. *Phys. Chem. Chem. Phys.* **2009**, *11*, 10245-10265.

3. Kvamme, B.; Kuznetsova, T.; Aasoldsen, K. Molecular Dynamics Simulations for Selection of Kinetic Hydrate Inhibitors. *J. Mol. Graph. Model.* **2005**, *23*, 524-536.

4. Forzatti, P.; Lietti, L. Catalyst Deactivation. *Catal. Today* **1999**, *52*, 165-181.

5. Xiao, Y.; Wang, S.; Wu, D.; Yuan, Q. Catalytic Oxidation of Hydrogen Sulfide over Unmodified and Impregnated Activated Carbon. *Sep. Purif. Technol.* **2008**, *59*, 326-332.

6. Chialvo, A. A.; Vlcek, L.; Cole, D. R. Acid Gases in CO_2-Rich Subsurface Geologic Environments. *Rev. Mineral. Geochem.* **2013**, *77*, 361-398.

7. Wang, X.; Ma, X.; Xu, X.; Sun, L.; Song, C. Mesoporous-Molecular-Sieve-Supported Polymer Sorbents for Removing H_2S from Hydrogen Gas Streams. *Top. Catal.* **2008**, *49*, 108-117.

8. Robb, W. L. Thin Silicone Membranes-Their Permeation Properties and Some Applications. *Ann. N. Y. Acad. Sci.* **1968**, *146*, 119-137.

9. Huang, H. Y.; Yang, R. T.; Chinn, D.; Munson, C. L. Amine-Grafted MCM-48 and Silica Xerogel as Superior Sorbents for Acidic Gas Removal from Natural Gas. *Ind. Eng. Chem. Res.* **2003**, *42*, 2427-2433.

10. Phan, A.; Cole, D. R.; Weiß, R. G.; Dzubiella, J.; Striolo, A. Confined Water Determines Transport Properties of Guest Molecules in Narrow Pores. *ACS Nano* **2016**, *10*, 7646-7656.

11. Argyris, D.; Tummala, N. R.; Striolo, A.; Cole, D. R. Molecular Structure and Dynamics in Thin Water Films at the Silica and Graphite Surfaces. *J. Phys. Chem. C* **2008**, *112*, 13587-13599.

12. Gerstberger, G.; Anwander, R. Screening of Rare Earth Metal Grafted Mcm-41 Silica for Asymmetric Catalysis. *Micropor. Mesopor. Mat.* **2001**, *44*, 303-310.

13. Donaldson, D. J.; Valsaraj, K. T. Adsorption and Reaction of Trace Gas-Phase Organic Compounds on Atmospheric Water Film Surfaces: A Critical Review. *Environ. Sci.Technol* **2010**, *44*, 865-873.

14. Hensen, E. J. M.; Smit, B. Why Clays Swell. *J. Phys. Chem. B* **2002**, *106*, 12664-12667.

15. Hu, Y.; Huang, L.; Zhao, S.; Liu, H.; Gubbins, K. E. Effect of Confinement in Nano-Porous Materials on the Solubility of a Supercritical Gas. *Mol. Phys.* **2016**, *114*, 3294-3306.

16. Le, T. T. B.; Striolo, A.; Gautam, S.; Cole, D. R. Propane-Water Mixtures Confined within Cylindrical Silica Nano-Pores: Structural and Dynamical Properties Probed by Molecular Dynamics. *Langmuir* **2017**, *33*, 11310-11320.

17. Argyris, D.; Cole, D. R.; Striolo, A. Hydration Structure on Crystalline Silica Substrates. *Langmuir* **2009**, *25*, 8025-8035.

18. Le, T.; Striolo, A.; Cole, D. R. CO_2–C_4H_{10} Mixtures Simulated in Silica Slit Pores: Relation between Structure and Dynamics. *J. Phys. Chem. C* **2015**, *119*, 15274-15284.

19. Striolo, A. From Interfacial Water to Macroscopic Observables: A Review. *Adsorpt. Sci. Technol.* **2011**, *29*, 211-258.

20. Phan, A.; Cole, D. R.; Striolo, A. Aqueous Methane in Slit-Shaped Silica Nanopores: High Solubility and Traces of Hydrates. *J. Phys. Chem. C* **2014**, *118*, 4860-4868.

21. Ho, L. N.; Clauzier, S. p.; Schuurman, Y.; Farrusseng, D.; Coasne, B. Gas Uptake in Solvents Confined in Mesopores: Adsorption Versus Enhanced Solubility. *J. Phys. Chem. Lett.* **2013**, *4*, 2274-2278.

22. Ho, L. N.; Schuurman, Y.; Farrusseng, D.; Coasne, B. Solubility of Gases in Water Confined in Nanoporous Materials: ZSM-5, MCM-41, and MIL-100. *J. Phys. Chem. C* **2015**, *119*, 21547-21554.

23. Diaz Campos, M.; Akkutlu, I. Y.; Sigal, R. F. In *A Molecular Dynamics Study on Natural Gas Solubility Enhancement in Water Confined to Small Pores*, SPE Annual Technical Conference and Exhibition, New Orleans, LA, Oct 4-7; Society of Petroleum Engineers: New Orleans, LA, 2009.

24. Luzar, A.; Bratko, D. Gas Solubility in Hydrophobic Confinement. *J. Phys. Chem. B* **2005**, *109*, 22545-22552.

25. Bratko, D.; Luzar, A. Attractive Surface Force in the Presence of Dissolved Gas: A Molecular Approach. *Langmuir* **2008**, *24*, 1247-1253.

26. Pera-Titus, M.; El-Chahal, R.; Rakotovao, V.; Daniel, C.; Miachon, S.; Dalmon, J. A. Direct Volumetric Measurement of Gas Oversolubility in Nanoliquids: Beyond Henry's Law. *ChemPhysChem* **2009**, *10*, 2082-2089.

27. Rakotovao, V.; Ammar, R.; Miachon, S.; Pera-Titus, M. Influence of the Mesoconfining Solid on Gas Oversolubility in Nanoliquids. *Chem. Phys. Lett.* **2010**, *485*, 299-303.

28. Gadikota, G.; Dazas, B.; Rother, G.; Cheshire, M. C.; Bourg, I. C. Hydrophobic Solvation of Gases (CO_2, CH_4, H_2, Noble Gases) in Clay Interlayer Nanopores. *J. Phys. Chem. C* **2017**, *121*, 26539-26550.

29. Riahi, S.; Rowley, C. N. Solvation of Hydrogen Sulfide in Liquid Water and at the Water–Vapor Interface Using a Polarizable Force Field. *J. Phys. Chem. B* **2014**, *118*, 1373-1380.

30. Lee, J.; Aluru, N. R. Water-Solubility-Driven Separation of Gases Using Graphene Membrane. *J. Membr. Sci.* **2013**, *428*, 546-553.

31. Golebiowska, M.; Roth, M.; Firlej, L.; Kuchta, B.; Wexler, C. The Reversibility of the Adsorption of Methane–Methyl Mercaptan Mixtures in Nanoporous Carbon. *Carbon* **2012**, *50*, 225-234.

32. Kalluri, R. K.; Konatham, D.; Striolo, A. Aqueous Nacl Solutions within Charged Carbon-Slit Pores: Partition Coefficients and Density Distributions from Molecular Dynamics Simulations. *J. Phys. Chem. C* **2011**, *115*, 13786-13795.

33. Guillot, B. A Reappraisal of What We Have Learnt During Three Decades of Computer Simulations on Water. *J. Mol. Liq.* **2002**, *101*, 219-260.

34. Kamath, G.; Potoff, J. J. Monte Carlo Predictions for the Phase Behavior of H_2S+N-Alkane, H_2S+ CO_2, CO_2+CH_4 and H_2S+CO_2+CH_4 Mixtures. *Fluid Phase Equilibr.* **2006**, *246*, 71-78.

35. Cygan, R. T.; Liang, J.J.; Kalinichev, A. G. Molecular Models of Hydroxide, Oxyhydroxide, and Clay Phases and the Development of a General Force Field. *J. Phys. Chem. B* **2004**, *108*, 1255-1266.

36. Allen, M. P.; Tildesley, D. J. *Computer Simulation of Liquids*; Oxford University Press: Oxford, UK, 2004.

37. Essmann, U.; Perera, L.; Berkowitz, M. L.; Darden, T.; Lee, H.; Pedersen, L. G. A Smooth Particle Mesh Ewald Method. *J. Chem. Phys.* **1995**, *103*, 8577-8593.

38. Abraham, M. J.; Murtola, T.; Schulz, R.; Páll, S.; Smith, J. C.; Hess, B.; Lindahl, E. Gromacs: High Performance Molecular Simulations through Multi-Level Parallelism from Laptops to Supercomputers. *SoftwareX* **2015**, *1*, 19-25.

39. Van Der Spoel, D.; Lindahl, E.; Hess, B.; Groenhof, G.; Mark, A. E.; Berendsen, H. J. C. Gromacs: Fast, Flexible, and Free. *J. Comput. Chem.* **2005**, *26*, 1701-1718.

40. Hockney, R. W.; Goel, S. P.; Eastwood, J. W. Quiet High-Resolution Computer Models of a Plasma. *J. Comput. Phys.* **1974**, *14*, 148-158.

41. Hoover, W. G. Canonical Dynamics: Equilibrium Phase-Space Distributions. *Phys. Rev. A* **1985**, *31*, 1695-1697.

42. Nosé, S. A Molecular Dynamics Method for Simulations in the Canonical Ensemble. *Mol. Phys.* **1984**, *52*, 255-268.

43. Miyamoto, S.; Kollman, P. A. Settle: An Analytical Version of the Shake and Rattle Algorithm for Rigid Water Models. *J. Comput. Chem.* **1992**, *13*, 952-962.

44. Kuranov, G.; Rumpf, B.; Smirnova, N. A.; Maurer, G. Solubility of Single Gases Carbon Dioxide and Hydrogen Sulfide in Aqueous Solutions of N-Methyldiethanolamine in the Temperature Range 313− 413 K at Pressures up to 5 Mpa. *Ind. Eng. Chem. Res.* **1996**, *35*, 1959-1966.

45. Wright, R. H.; Maass, O. The Solubility of Hydrogen Sulphide in Water from the Vapor Pressures of the Solutions. *Can. J. Res.* **1932**, *6*, 94-101.

46. Selleck, F. T.; Carmichael, L. T.; Sage, B. H. Phase Behavior in the Hydrogen Sulfide-Water System. *Ind. Eng. Chem.* **1952**, *44*, 2219-2226.

47. Lee, J. I.; Mather, A. E. Solubility of Hydrogen Sulfide in Water. *Ber. Bunsenges. Phys. Chem.* **1977**, *81*, 1020-1023.

48. Clarke, E. C. W.; Glew, D. N. Aqueous Nonelectrolyte Solutions. Part Viii. Deuterium and Hydrogen Sulfides Solubilities in Deuterium Oxide and Water. *Can. J. Chem.* **1971**, *49*, 691-698.

49. Gillespie, P. C.; Owens, J. L.; Wilson, G. M. In *Sour Water Equilibria Extended to High Temperatures and with Inerts Present*, AIChE Winter National Meeting, Atlanta, GA, March 11-14; 1984.

50. Kirkwood, J. G.; Buff, F. P. The Statistical Mechanical Theory of Surface Tension. *J. Chem. Phys.* **1949**, *17*, 338-343.

51. Shah, V.; Broseta, D.; Mouronval, G.; Montel, F. Water/Acid Gas Interfacial Tensions and Their Impact on Acid Gas Geological Storage. *Int. J. GreenH Gas Con.* **2008**, *2*, 594-604.

52. Míguez, J. M.; Piñeiro, M. M.; Blas, F. J. Influence of the Long-Range Corrections on the Interfacial Properties of Molecular Models Using Monte Carlo Simulation. *J. Chem. Phys.* **2013**, *138*, No. 034707.

53. Taylor, R. S.; Dang, L. X.; Garrett, B. C. Molecular Dynamics Simulations of the Liquid/Vapor Interface of SPC/E Water. *J. Phys. Chem.* **1996**, *100*, 11720-11725.

54. VandeVondele, J.; Krack, M.; Mohamed, F.; Parrinello, M.; Chassaing, T.; Hutter, J. Quickstep: Fast and Accurate Density Functional Calculations Using a Mixed Gaussian and Plane Waves Approach. *Comput. Phys. Commun.* **2005**, *167*, 103-128.

55. Mark, P.; Nilsson, L. Structure and Dynamics of the TIP3P, SPC, and SPC/E Water Models at 298 K. *J. Phys. Chem. A* **2001**, *105*, 9954-9960.

56. Tamimi, A.; Rinker, E. B.; Sandall, O. C. Diffusion Coefficients for Hydrogen Sulfide, Carbon Dioxide, and Nitrous Oxide in Water over the Temperature Range 293-368 K. *J. Chem. Eng. Data* **1994**, *39*, 330-332.

57. Ho, T. A.; Argyris, D.; Papavassiliou, D. V.; Striolo, A.; Lee, L. L.; Cole, D. R. Interfacial Water on Crystalline Silica: A Comparative Molecular Dynamics Simulation Study. *Mol. Simul.* **2011**, *37*, 172-195.

58. Malani, A.; Ayappa, K. G.; Murad, S. Effect of Confinement on the Hydration and Solubility of Nacl in Water. *Chem. Phys. Lett.* **2006**, *431*, 88-93.

59. Gowers, R. J.; Linke, M.; Barnoud, J.; Reddy, T. J. E.; Melo, M. N.; Seyler, S. L.; Dotson, D. L.; Domanski, J.; Buchoux, S.; Kenney, I. M. In *Mdanalysis: A Python Package for the Rapid Analysis of Molecular Dynamics Simulations*, Proceedings of the 15th Python in Science Conference, Austin, TX, Benthall, S., Ed. SciPy: Austin, TX, 2016.

60. Michaud-Agrawal, N.; Denning, E. J.; Woolf, T. B.; Beckstein, O. Mdanalysis: A Toolkit for the Analysis of Molecular Dynamics Simulations. *J. Comput. Chem.* **2011**, *32*, 2319-2327.

61. Kinaci, A.; Haskins, J. B.; Çağın, T. On Calculation of Thermal Conductivity from Einstein Relation in Equilibrium Molecular Dynamics. *J. Chem. Phys.* **2012**, *137*, No. 014106.

62. Hansen, E. W.; Schmidt, R.; Stöcker, M.; Akporiaye, D. Self-Diffusion Coefficient of Water Confined in Mesoporous MCM-41 Materials Determined by 1H Nuclear Magnetic Resonance Spin-Echo Measurements. *Micropor. Mat.* **1995**, *5*, 143-150.

63. Ringnér, M. What Is Principal Component Analysis? *Nat. Biotechnol* **2008**, *26*, 303-304.

64. Bui, T.; Phan, A.; Cole, D. R.; Striolo, A. Transport Mechanism of Guest Methane in Water-Filled Nano-Pores. *J. Phys. Chem. C* **2017**, *121*, 15675-15686.

65. Liu, H.; Dai, S.; Jiang, D. Molecular Dynamics Simulation of Anion Effect on Solubility, Diffusivity, and Permeability of Carbon Dioxide in Ionic Liquids. *Ind. Eng. Chem. Res.* **2014**, *53*, 10485-10490.

66. Argyris, D.; Cole, D. R.; Striolo, A. Dynamic Behavior of Interfacial Water at the Silica Surface. *J. Phys. Chem. C* **2009**, *113*, 19591-19600.

67. Phan, A.; Cole, D. R.; Striolo, A. Preferential Adsorption from Liquid Water–Ethanol Mixtures in Alumina Pores. *Langmuir* **2014**, *30*, 8066-8077.

TOC Graphic